Available online at www.sciencedirect.com
ScienceDirect
Catalysis Today 118 (2006) 12–23
CATALYSIS TODAY
www.elsevier.com/locate/cattod

Dense inorganic membranes for production of hydrogen from methane and coal with carbon dioxide sequestration

M.V. Mundschau *, X. Xie, C.R. Evenson IV, A.F. Sammells

Eltron Research Inc., 4600 Nautilus Court South, Boulder, CO 80301-3241, United States

Available online 3 July 2006

Abstract

Principles and strategies for design and operation of catalysts associated with both dense oxygen transport membranes and dense hydrogen transport membranes are discussed. Dense ceramic oxygen transport membranes function through the diffusion of oxygen anions, O^{2-}. A key catalytic step is the adsorption and dissociation of molecular oxygen, and the associated transfer of four electrons. In dense hydrogen transport membranes, whether ceramic or metallic, molecular hydrogen must be catalytically dissociated on the retentate-side membrane surface to allow transport of hydrogen through the bulk membrane in a dissociated form. Dissociated hydrogen must be re-combined and desorbed from the permeate side membrane surface. Strategies are discussed for increasing resistance of catalysts to poisons. By separating oxygen from the other components of air, oxygen transport membranes allow a potential efficient means for production of synthesis gas ($H_2 + CO$) from natural gas or coal, without diluting the product with nitrogen. Further reaction of CO with steam over water-gas shift catalysts produces additional hydrogen plus CO_2. Extraction of hydrogen from water-gas shift reactors through dense hydrogen transport membranes, while retaining CO_2 at operating pressures of coal gasifiers (e.g. 1000 psi or 69 bar) produces essentially pure hydrogen in the permeate and CO_2 at high pressure and high concentration, which is ideal for efficient sequestration of CO_2. Process flow scenarios for integration of both oxygen transport membranes and hydrogen transport membranes with coal gasifiers, natural gas syngas reactors, water-gas shift reactors and systems for sequestration of CO_2 are discussed.

Keywords: Sequestration; Water-gas shift reactor; Oxygen transport membranes

1. Introduction

This paper emphasizes some of the aspects of catalysis relating to both oxygen ion transport membranes and dense hydrogen purification membranes. The catalytic reactions and strategy used to convert methane (CH_4) into synthesis gas ($H_2 + CO$) are discussed for dense oxygen ion transport membranes. For dense hydrogen transport membranes, which are used to extract and purify hydrogen from reaction mixtures, issues are discussed relating to selection and design of hydrogen dissociation catalysts. For the integration of membranes with coal gasifiers, which are also used for the production of synthesis gas and hydrogen, critical issues relating to prevention of poisoning of membrane catalysts are reviewed.

2. Catalysis on oxygen transport membranes for reforming of methane

Fig. 1 shows schematically some of the chemical reactions occurring during conversion of methane into synthesis gas using dense mixed oxygen-ion and electron conducting membranes. Common membranes use materials with the perovskite crystal structure (Fig. 2) [1–3]. Perovskites have also long been used in oxidation catalysts [4,5]. Perovskite materials are designed to contain a large number of vacancies at oxygen lattice sites. These empty lattice sites, which allow oxygen anions to hop from site to site, increase oxygen anion mobility in the crystal lattice. Oxygen anion mobility is desired in both oxygen transport membranes and in oxidation catalysts. For charge balance, the perovskite materials are also designed to be good conductors of electrons.

Oxygen vacancies in the bulk crystal lattice of perovskites containing metal ions with formal charges of 3^+, for example, are increased by doping with metal ions possessing lower

* Corresponding author. Tel.: +1 303 530 0263; fax: +1 303 530 0264.
E-mail address: mundschau@eltronresearch.com (M.V. Mundschau).

0920-5861/$ – see front matter © 2006 Elsevier B.V. All rights reserved.
doi:10.1016/j.cattod.2006.01.042

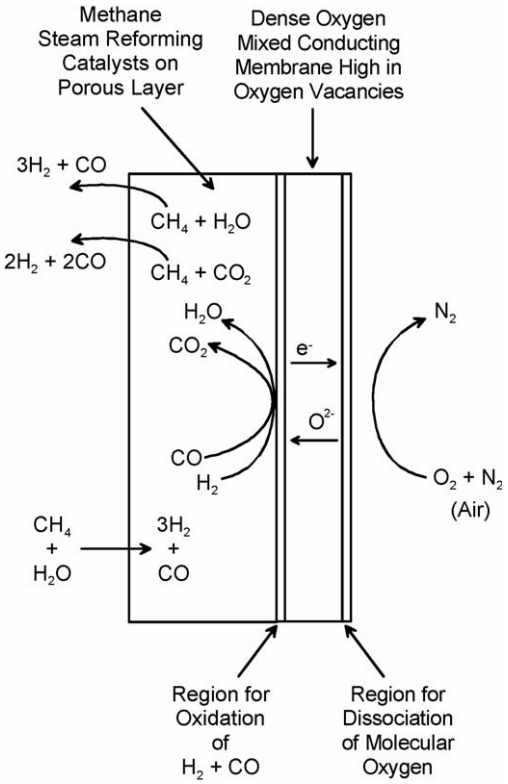

Fig. 1. Schematic of oxygen transport membrane system for conversion of methane into synthesis gas. Endothermic reforming reactions in a porous layer are driven by exothermic oxidation reactions at the dense membrane surface. Oxygen is separated from the other components in air though the dense membrane.

formal charges of 2^+. The net lower total positive charge of the cations in the lattice requires less oxygen of formal charge 2^- needed for charge balance. This results in increased numbers of oxygen vacancies in the charge-neutral crystal structure. Electron conductivity is enhanced by doping B-sites with metallic elements possessing multiple valence, such as Fe^{2+}, Fe^{3+}; Co^{2+}, Co^{3+}, etc. [6–8].

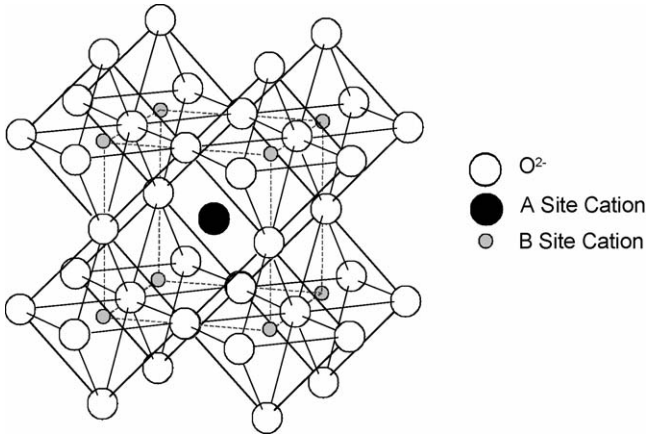

Fig. 2. Perovskite crystal structure of materials used in common oxygen transport membranes and oxidation catalysts. Large cations such as La^{3+}, Ca^{2+}, and Sr^{2+} occupy the A-sites. Smaller cations, with multiple valence essential for electron conduction, occupy the B-sites and often include ions of Ni, Fe, Co, Mn, and Cr.

Oxygen vacancies in both the crystal bulk as well as on the crystal surfaces are critical for function of the catalytic membrane reactors based on perovskite-type membranes. Molecular oxygen likely adsorbs and dissociates at oxygen vacancy sites on the air side surface of the membranes. Electron conduction in the membrane material is essential for the four-electron reduction of molecular oxygen. Henrich and Cox [9] present models of the perovskite (1 0 0) and (1 1 1) surfaces determined by low-energy electron diffraction (LEED). The models of Henrich and Cox aid in the visualization of surface oxygen vacancy sites on perovskites and other possible active sites for catalysis [9].

In practical functioning catalytic membrane reactors used for the conversion of methane, the major reaction steps are as follows. Methane is initially steam reformed in a porous layer of perovskite material, which is sintered to a dense oxygen transport perovskite membrane of the same material, as shown schematically in Fig. 1. Steam reforming catalysts are dispersed in the perovskite porous material and convert methane and steam into synthesis gas: $CH_4 + H_2O\,(g) = 3H_2 + CO$. This steam reforming step is highly endothermic, with $\Delta H = +206\ \mathrm{kJ\ mol^{-1}}$ [10]. Although nickel is a standard methane steam reforming catalyst used in industry [10], nickel, in general, is not used with the perovskite-based membranes because of issues with interdiffusion at membrane operating temperatures between 900 and 1000 °C. Noble metals from the platinum group are preferred in steam reforming catalysts used in the porous layers of perovskite.

Molecular hydrogen (and to a lesser extent CO) formed during the initial steam reforming steps, diffuses through the porous layer to the fuel-side surface of the dense perovskite membrane. The molecular hydrogen (and CO) reacts with and extracts oxygen from surface lattice sites to form steam (and CO_2), and create oxygen vacancies on the membrane surface. The surface vacancies so created provide empty sites into which jump oxygen anions, O^{2-}, from deeper in the crystal lattice. The hopping of the oxygen anions continues throughout the membrane lattice until the oxygen vacancies appear on the air side surface of the dense membrane. These surface vacancies are filled by adsorption and dissociation of molecular oxygen, which is, thus, separated from nitrogen and the other components of air.

The major net oxidation reactions across the membrane are:

$$H_2 + (1/2)O_2 = H_2O(g), \quad \Delta H = -241.818\ \mathrm{kJ\ mol^{-1}}$$

$$CO + (1/2)O_2 = CO_2, \quad \Delta H = -393.509\ \mathrm{kJ\ mol^{-1}}$$

These highly exothermic reactions provide heat within the porous layer to drive the endothermic steam reforming reaction as well as reforming of CO_2:

$$CO_2 + CH_4 = 2H_2 + 2CO; \quad \Delta H = +247.269\ \mathrm{kJ\ mol^{-1}}.$$

No special effort is made to produce catalysts for the difficult direct partial oxidation of methane, nor are such catalysts necessary for the successful operation of the membranes. Instead, membranes are operated in the thermodynamic regime which overwhelmingly favors the production of $H_2 + CO$, rather than deep oxidation of methane to $H_2O + CO_2$. Fig. 3

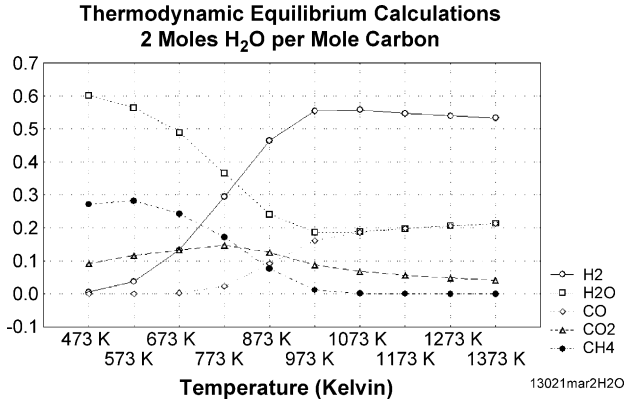

Fig. 3. Thermodynamic equilibrium calculations for mole fractions vs. temperature showing that $H_2 + CO$ are the overwhelmingly favored products at temperatures above about 1173 K (900 °C) when the atomic ratio of H:C:O is 4:1:1. Special catalysts for direct partial oxidation of methane are not necessary in membrane reactors operating at these equilibrium conditions.

plots results of thermodynamic equilibrium calculations showing the relative mole fractions produced of the desired H_2 and CO, and the undesired deep oxidation products, H_2O and CO_2, as a function of temperature. The plot is for atomic ratios of H:C:O of 4:1:1, which allows good product yield and essentially zero deposition of carbon with minimum use of steam.

For temperatures above about 900 °C (1173 K), Fig. 3 shows that H_2 and CO are the thermodynamically preferred products, and that steam and CO_2 will be consumed if the reactions are brought to equilibrium. Even if deep oxidation to H_2O and CO_2 occurs initially at the dense membrane surface, these undesired products cannot remain stable in the porous layer at equilibrium and will react with other components of the gas mixture to form the desired $H_2 + CO$. This will occur as long as the atomic ratios in the reaction mixture are carefully controlled, and if the catalysts in the porous layer allow kinetics sufficient for equilibrium to be achieved before molecules diffuse out of the porous layers. Feeds of methane and steam must be matched with oxygen flux through the membrane to balance the heat consumed by the endothermic reactions with that produced by the exothermic reactions.

Not plotted in Fig. 3 is the formation of carbon, which is absolutely negligible above 850 °C for these equilibrium conditions. The atomic ratios of H:C:O of 4:1:1 were especially chosen to eliminate deposition of carbon at the higher reaction temperatures. It is imperative to seek reaction conditions which avoid deposition of carbon, which otherwise will poison the steam reforming catalysts.

In the latest generation of oxygen transport membrane materials, intrinsic catalytic activity especially for oxidation of H_2 at the dense membrane fuel side surface, and activity for adsorption and dissociation of molecular oxygen on the dense air side surface are sufficient so that no additional oxidation catalysts or oxygen dissociation catalysts are required. In earlier membrane systems, palladium, $LaSrCoO_{3-x}$, or Pd mixed with $LaSrCoO_{3-x}$, were used as catalysts on the air side of the membranes to enhance adsorption and dissociation of molecular oxygen. In the case of dense membranes coated with relatively thick porous catalytic layers, for which diffusion of products out of the porous layer is rate limiting, catalysts for enhancing oxygen adsorption and dissociation on the membrane air side are not necessary or desired. Elimination of such oxygen dissociation catalysts removes potential issues of interdiffusion of the catalysts with the bulk membrane materials at the high temperatures (>900 °C) employed.

3. Integration of oxygen and hydrogen transport membranes in systems for the production of pure hydrogen

Fig. 4 shows possible scenarios for integrating both oxygen transport membranes and hydrogen separation membranes with systems for using natural gas or coal to produce pure hydrogen. Fig. 4a shows a possible system for producing very pure hydrogen from natural gas. As the first step, sulfur-containing odorants and other potential catalyst poisons are removed from pipeline natural gas using conventional liquid absorbents operating at ambient or low temperatures. The clean natural gas is then mixed with steam and heated to 950 °C and passed over the fuel side of the oxygen ion transport membrane. Likewise air is heated to 950 °C and passed over the air side of the membrane. The steam reforming and oxidation reactions convert natural gas into $H_2 + CO$, which is then cooled to 320 °C in a heat exchanger, which heats the original air, steam and natural gas to the membrane operating temperature. In the water-gas shift reactor operating between 320 and 440 °C, the CO is reacted with additional steam to produce CO_2 and additional hydrogen. Hydrogen is extracted through the hydrogen separation membrane at essentially 100% selectivity to produce hydrogen of sufficient purity for operation of proton exchange membrane fuel cells, for example. Such a system might be used to produce electricity in remote sites where natural gas (or propane) is readily available but which is not connected to the electric power grid or for more efficient production of electricity at stationary residential or small business power sites operating on natural gas.

In the gasification of coal by steam and oxygen (Fig. 4b), it is highly desired to integrate oxygen separation units to avoid diluting the syngas product stream with nitrogen. This is especially true if CO_2 is to be sequestered [11]. If oxygen transport membranes are to be used as the oxygen separation unit, a likely scenario is that gaseous reactants originating from coal will be used to react with oxygen on the membrane fuel side surfaces and thus aid diffusion of oxygen through the membranes. Part of the carbon in coal (or its volatile components) will be first steam reformed. Part of the hydrogen or the syngas stream will be recirculated to the membrane (not shown in Fig. 4b). As in the case of methane reforming, the H_2 (and to a lesser extent, CO) will react with the oxygen in the membrane surface to form steam and CO_2 plus heat. The hot steam and CO_2 from the membrane will then be fed back to the coal gasifier where the hot H_2O plus CO_2 will react with the carbon in coal to form $H_2 + CO$, which are the favored equilibrium products under gasifier reaction conditions.

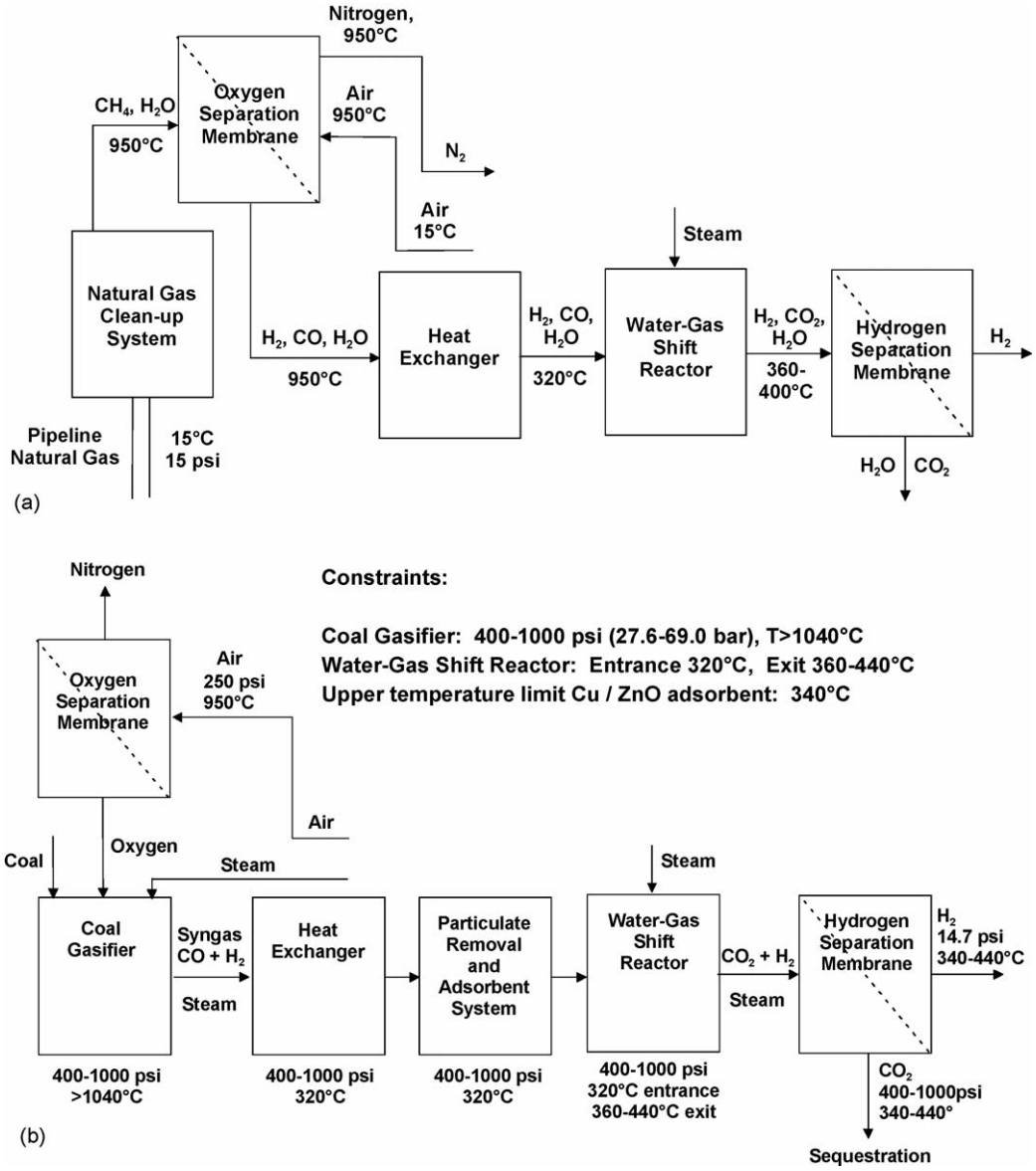

Fig. 4. (a) System for producing ultra-high purity hydrogen from natural gas, integrating both oxygen transport and hydrogen separation membranes. (b) Possible process flow scenario for integrating both oxygen transport membranes and hydrogen purification membranes with coal gasifiers for production of hydrogen and sequestration of CO_2.

Commercial coal gasifiers typically operate at 400 or 1000 psi (27.6 or 69.0 bar) and temperatures greater than 1040 °C. If CO_2 is to be sequestered, it is highly desirable that hydrogen transport membranes downstream retain the CO_2 at the gasifier pressure to minimize downstream compression costs for CO_2. The critical pressure needed to liquefy CO_2 for convenient transport and sequestration is 73.9 bar (1071 psi) [12]. Pressures well in excess of this (>2000 psi) are required, however, to force the CO_2 into oil wells or other underground storage sites.

If hydrogen is to be the main product, then it is highly desired to use low-cost, commercial high-temperature water-gas shift catalysts. According to Twigg et al. [10], commercial catalysts based upon Fe_3O_4/Cr_2O_3 typically operate with inlet temperatures near 320 °C, depending upon catalyst age and activity. With this temperature constraint, the syngas emerging from the coal gasifier at >1040 °C, must be cooled to 320 °C. A heat exchanger can be used to recover much of the thermal energy and to raise the temperature of steam, air, or oxygen, required for coal gasification.

Syngas at 320 °C will allow installation of fairly conventional particulate removal systems, necessary to protect the bed of water-gas shift catalyst from the myriad of particulate matter which can originate from coal [13]. A fraction of the coal-derived impurities, which are volatile at 1040 °C, will likely condense on the surface of the trapped particulates at 320 °C. However, a warm-gas clean-up system containing high-surface area adsorbents such as Cu/ZnO or $ZnTiO_3$ to partially remove sulfur and other contaminants will be required to protect catalysts downstream. For natural gas, clean-up can be performed at room temperature before reforming, using standard gas absorption techniques.

The exothermic water-gas shift reaction (H_2O (g) + CO = H_2 + CO_2; $\Delta H = -41.1$ kJ mol^{-1}) raises exit temperatures of high-temperature water-gas shift reactors typically to between 360 and 440 °C, again depending upon the age and activity of the catalysts [10]. According to Twigg et al. temperatures in the bed of high-temperature water-gas shift catalysts should not exceed 440 °C in order to avoid sintering of the high-surface area catalysts [10]. If hydrogen purification membranes are to be integrated with high-temperature water-gas shift reactors or placed immediately downstream from the catalyst bed, the membranes must be compatible with exhaust temperatures of approximately 360–440 °C, as well as high pressure steam, CO_2, 3–4 mol% residual CO which remains unconverted in the high-temperature water-gas shift reactor [10] and the residual impurities which escape the warm-gas clean-up system and bed of water-gas shift catalyst.

4. Catalysis issues in hydrogen transport membranes

All of the common dense hydrogen transport membranes, capable of essentially 100% selectivity for hydrogen, transport hydrogen in a dissociated form [14]. These systems include palladium, alloys of palladium (such as Pd–Ag and Pd–Cu), the superpermeable elements (such as niobium, tantalum, vanadium and zirconium and their alloys), cermets (ceramic–metals) fabricated by sintering together hydrogen permeable metals and ceramics, and the proton conducting ceramics [4]. Because hydrogen is transported in a dissociated form (i.e. as protons (H^+), hydride ions (H^{1-}), neutral atoms, or neutral proton–electron pairs [14]), this implies that molecular hydrogen must be adsorbed and dissociated on the hydrogen feed (retentate) side of the membrane and recombined and desorbed on the hydrogen sink (permeate) side of the membrane (see Fig. 5).

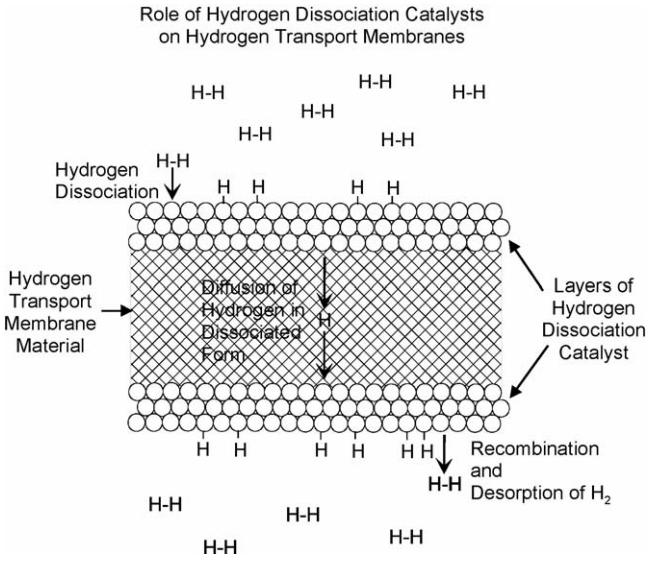

Fig. 5. Schematic showing the role of hydrogen dissociation catalysts on both surfaces of dense membranes which transport hydrogen in a dissociated form. Catalysts must be optimized for adsorption of hydrogen and resistance to impurities on the hydrogen source side (top), and optimized for desorption of hydrogen on the hydrogen sink side (bottom).

Table 1
Initial heats of adsorption of hydrogen and CO on various metal surfaces

Surface	Hydrogen (kJ mol^{-1})	CO (kJ mol^{-1})
Ag (1 1 1)	74	25
Cu (1 0 0)	85	58
Co (0 0 0 1)	80	105
Ni (1 1 1)	96	111
Pt (1 1 1)	84	126
Ru (0 0 0 1)	80	160
Pd (1 1 1)	88	142
Pd (1 0 0)	102	161

Data adapted from Christmann [15] and Benzinger [16].

For elements such as palladium, which have intrinsic catalytic activity for the adsorption and dissociation of molecular hydrogen, no additional catalyst may be needed. However, for membrane materials such as Nb, Ta, V, and Zr, which rapidly form oxides, carbides and nitrides, which poison the hydrogen dissociation reaction and which block permeation of hydrogen, noble metal catalysts, in general, must be applied to both membrane surfaces. The hydrogen dissociation catalysts on the retentate surface must protect the underlying membrane materials from components of the feed and must be made resistant to the level of catalyst poisons remaining downstream from the water-gas shift or other reactors. Catalysts on the permeate side should be optimized for hydrogen desorption.

In the design and selection of catalysts for hydrogen transport membranes which will be operated in feed gas mixtures containing a few mole percent residual carbon monoxide, as is the case downstream from high-temperature water-gas shift reactors, it is instructive to consider the relative heats of adsorption of hydrogen and CO for various candidate catalytic materials. Initial heats of adsorption for hydrogen and CO, as adapted from work of Christmann [15] and Benzinger [16] are listed in Table 1.

For desired strong adsorption of molecular hydrogen on feed side membrane surfaces, palladium with its relatively high heat of adsorption for hydrogen (88–102 kJ mol^{-1}) might make the best hydrogen adsorption and dissociation catalyst. On the hydrogen permeate side of the membranes, however, where desorption of molecular hydrogen is required, silver might be the best choice due to its low heat of adsorption of 74 kJ mol^{-1}. In practice, alloys of 75 at.% Pd and 25 at.% Ag (which also have the highest permeability for hydrogen of the Pd–Ag alloys [17]) appear optimum and take advantage of the hydrogen adsorption/desorption properties of palladium and silver. For resistance to competitive adsorption between CO and H_2, silver and copper, with their relatively low heats of adsorption for CO of 25 and 58 kJ mol^{-1}, respectively, might provide advantages on the hydrogen source side of membranes exposed to mixtures containing H_2 and CO.

Fig. 6 shows the performance of an unalloyed palladium membrane, 100 μm thick, at ambient pressure exposed to a simulated high-temperature water-gas shift exhaust containing 41 mol% H_2, 3.3 mol% CO, 17.8 mol% CO_2, 37.3 mol% steam, and balance of inert gases. The first data points for each

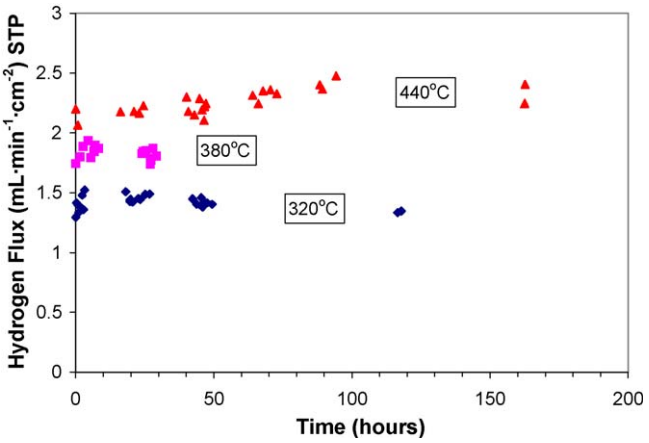

Fig. 6. Performance of unalloyed palladium membranes (100 μm thick) at ambient pressure in water-gas shift mixtures containing 41 mol% H_2, 3.3 mol% CO, 17.8 mol% CO_2, and 37 mol% H_2O with balance of inert gases. First data points for each series on the vertical axis are for ideal hydrogen/helium mixtures. Data show that the water-gas shift mixture does not affect palladium for these conditions.

temperature series, on the vertical axis, show hydrogen flux data for ideal 41 mol% H_2/59 mol% He mixtures in the feed. The data show that the components of the water-gas shift mixture do not adversely affect the hydrogen flux relative to the ideal hydrogen/helium mixtures through relatively thick unalloyed palladium membranes in the high-temperature water-gas shift mixture of interest between 320 and 440 °C.

At much lower temperatures, a monolayer of CO will certainly form on palladium surfaces, occupying all surface adsorption sites and poisoning the adsorption and dissociation of molecular hydrogen. For temperatures above 320 °C, desorption of CO appears to be sufficient to allow adequate adsorption and dissociation of molecular hydrogen. It should also be noted that for thicker palladium membranes, in this case 100 μm, diffusion of dissociated hydrogen through the bulk palladium crystal lattice is the rate limiting step, and some loss

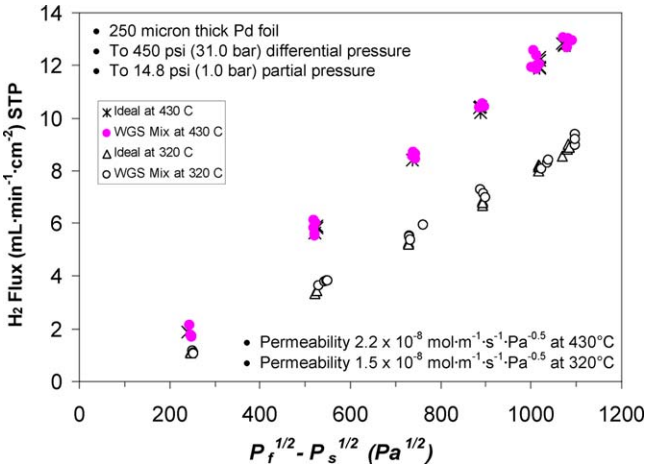

Fig. 7. Comparison of hydrogen flux through thick (250 μm) unalloyed palladium under ideal hydrogen/helium conditions and under simulated high-pressure water-gas shift conditions. The palladium is unaffected by the main components (CO, CO_2, steam) of the water-gas shift mixture.

of surface catalytic activity by adsorption of CO would not be detected at this membrane thickness. For very thin membranes of unalloyed palladium, surface catalysis can become the rate limiting step for hydrogen flux through palladium membranes, and in these cases some poisoning by CO, at the same conditions as discussed above, might become manifest.

Fig. 7 compares the performance of an unalloyed Pd foil, 250 μm thick, exposed to ideal hydrogen/helium mixtures and high-pressure water-gas shift mixtures of composition as described above at differential pressures up to 450 psi (31.0 bar). Fig. 7 shows that when hydrogen flux is plotted versus the difference in the square roots of the hydrogen partial pressures on either side of the membrane, the data fall on a straight line. This is in accord with Sieverts' Law [14] and implies that hydrogen diffuses through palladium in a dissociated form and that bulk diffusion through palladium is the rate-limiting step for this thickness (250 μm) of palladium foil.

Hydrogen flux was essentially identical for both the ideal and water-gas shift mixture (both containing the same partial pressure of hydrogen in the feed) up to the limits of the test to 450 psi (31.0 bar) differential pressure, for a feed containing up to 14.8 psi (1.0 bar) partial pressure of carbon monoxide. Permeability of the unalloyed palladium foil was 2.2×10^{-8} mol m^{-1} s^{-1} $Pa^{-0.5}$ at 430 °C and 1.5×10^{-8} mol m^{-1} s^{-1} $Pa^{-0.5}$ at 320 °C, in good agreement with literature values [14]. No poisoning of the palladium membrane was observed at CO partial pressures up to 1 bar for temperatures above 320 °C. For this thickness of palladium membrane (250 μm), which was necessary to resist the 31.0 bar differential pressure, possible partial poisoning of the surface by CO again may not be seen, because diffusion of dissociated hydrogen through the bulk palladium crystal lattice is the rate-limiting step for hydrogen flux.

It should be noted that the quantity of steam in the reaction mixture (37.3 mol%) was sufficient to prevent deposition of carbon on the surface. In dry mixtures or in mixtures with insufficient steam, the reaction: $2CO = C\ (s) + CO_2$ will poison the hydrogen dissociation reaction and block hydrogen flux. It should be noted that steam can corrode or react with poorly selected reactor wall materials, which if carried by steam and deposited onto membrane surfaces can poison palladium-based membranes. For unalloyed palladium, no carbonates should form to poison the catalytic surface. Oxides, such as PdO, are not thermodynamically stable under such reducing conditions and cannot poison surface reactions.

Recent studies on hydrogen transport membranes at Eltron Research Inc. have centered around use of composite membranes based upon elements such as Nb, Ta, V and Zr, which possess 10–100 times higher hydrogen permeability relative to unalloyed palladium [4,11]. Such materials are coated on both sides by hydrogen dissociation catalysts, typically palladium or its alloys [18]. Fig. 8 show hydrogen flux data through one such composite membrane exposed to various components of the water-gas shift mixture. The composite membrane was coated with 400 nm thick layers of unalloyed palladium on each side.

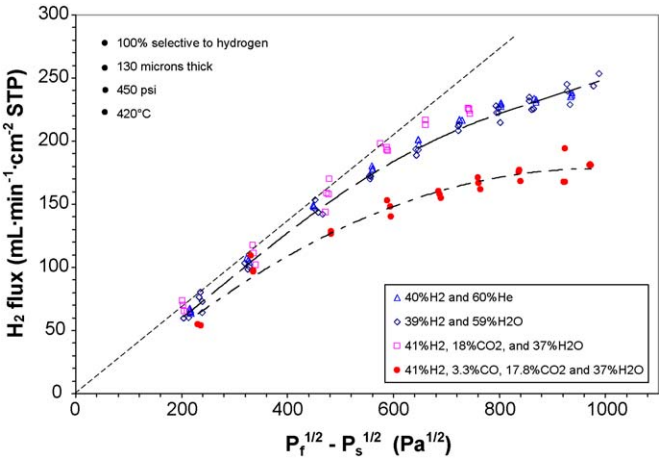

Fig. 8. Effect of components of the high-temperature water-gas shift mixture on 400 nm thick layers of unalloyed palladium catalysts vapor deposited onto composite membranes of Groups IVB–VB elements.

Under ideal 40 mol% H_2/60 mol% He mixtures, hydrogen flux of 250 mL min^{-1} cm^{-2} (STP) was achieved for a 130 μm thick membrane operated at 420 °C and a differential pressure of 31.0 bar. (Note the much greater hydrogen flux of the composite membrane of Fig. 8 relative to the unalloyed palladium membrane of Fig. 7, both of which are 100% selective to hydrogen.) Sieverts' Law was obeyed at lower total feed pressures, but deviations occurred as pressure was raised to 31.0 bar. This is attributed to gas phase diffusion limitations, as is proven by increasing concentration of hydrogen in the feed from 40 mol% to 60–90 mol%, which brings the data back to the Sieverts' Law line [4,11].

As shown in Fig. 8, replacement of most of the helium with steam or mixtures of steam and CO_2 does not affect hydrogen flux, demonstrating that these gases are inert to the palladium catalyst surface. Addition of 3.3 mol% CO, however, does diminish the hydrogen flux from a maximum near 250 mL min^{-1} cm^{-2} (STP) to 150–180 mL min^{-1} cm^{-2} (STP). This is attributed to competitive adsorption of CO with H_2 on palladium on the membrane feed surface. For this thickness of composite membrane (130 μm) and palladium catalyst (400 nm on each side), surface catalysis becomes rate limiting, as demonstrated in earlier work [11]. Partial poisoning of the palladium catalyst by adsorption of CO is now manifest, whereas it was not under similar feed conditions when diffusion through the bulk phase was the rate limiting step, and total hydrogen flux was less than 12 mL min^{-1} cm^{-2}, as in Fig. 7. From these studies it might be predicted that very thin films of palladium supported on porous substrates might also show partial poisoning by adsorption of CO if surface catalysis is the rate-limiting step. Despite partial poisoning of unalloyed palladium catalysts by adsorption of CO under the conditions studied, the composite membranes produce a very respectable hydrogen flux of over 150 mL min^{-1} cm^{-2} (STP) under simulated high-temperature water-gas shift conditions.

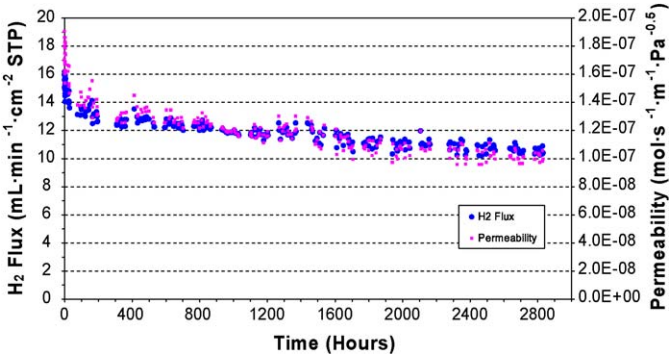

Fig. 9. Long-term test at 340 °C and ambient pressure with the full water-gas shift mixture containing 41.4 mol% H_2, 3.3% CO, 17.8% CO_2, 37.3% steam and balance of inert gases. After 4 months continuous operation, permeability remained at 1.0×10^{-7} mol m^{-1} s^{-1} $Pa^{-0.5}$, better than unalloyed palladium.

A composite membrane was tested at ambient pressure with a full mixture of water-gas shift containing 41.4% H_2, 3.3% CO, 17.8% CO_2, 37.3% steam and balance of inert gases in volume at 340 °C. The feed side reactor compartment was packed with low-temperature water-gas shift catalyst (Cu/ZnO obtained from Süd Chemie) as the guard bed. As shown in Fig. 9, the membrane displayed an initial hydrogen flux of approximately 14 mL min^{-1} cm^{-2} (STP), corresponding to an apparent hydrogen permeability of 1.4×10^{-7} mol m^{-1} s^{-1} $Pa^{-0.5}$. After 4 months (~2800 h) of continuous operation in the full water-gas shift mixture, the membrane maintained ~10 mL min^{-1} cm^{-2} (STP) of hydrogen flux and an apparent permeability of 1.0×10^{-7} mol m^{-1} s^{-1} $Pa^{-0.5}$.

5. Catalysts of palladium alloys and palladium intermetallic compounds on composite hydrogen transport membranes

Both theoretical and experimental work at Eltron Research Inc. suggest that performance of the composite membranes can be further improved by replacing unalloyed palladium catalysts with palladium alloys or palladium intermetallic compounds. For example, palladium–silver alloys of the high flux composition, 75 at.% Pd and 25 at.% Ag [17], will enhance hydrogen diffusion through the catalytic layers and enhance hydrogen desorption on the membrane permeate side. Alloys of Pd–Cu, for example, or other sulfur tolerant alloys or intermetallic compounds on the membrane retentate surface, could be used to resist sulfur if present in the hydrogen feed.

The preparation of thin films of palladium–silver alloys for use as hydrogen transport membranes is described extensively in the literature. Common methods for deposition of palladium–silver alloys include sputtering [19–21], electroless deposition [22,23], and vapor deposition [24]. At Eltron Research Inc. palladium–silver alloy catalysts are prepared by vapor deposition of alternating layers of palladium and silver followed by interdiffusion. Initially three layers were deposited (palladium, silver, palladium). The mass of each layer, as determined by a quartz crystal microbalance, was calculated to achieve a desired alloy composition of 75 at.% Pd and 25 at.% Ag with a target total thickness of 400 nm. Following deposition, palladium and silver are allowed to interdiffuse at elevated temperature. Temperatures were increased in steps

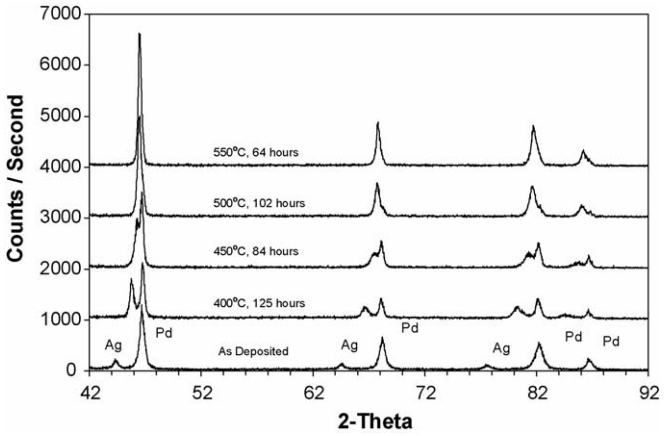

Fig. 10. X-ray diffraction data following the interdiffusion between alternating layers of vacuum vapor deposited palladium and silver to form a homogeneous 75 at.% Pd and 25 at.% Ag alloy.

to determine the lowest temperature necessary to form a homogeneous single phase alloy.

Fig. 10 shows X-ray diffraction data for the as deposited palladium and silver alternating layers and the changes which occur as interdiffusion progresses at temperatures of 400, 450, 500 and 550 °C. Distinct peaks assigned to elemental palladium and silver are seen in the as deposited sample. Heating for 125 h at 400 °C indicates that interdiffusion of palladium into silver occurs, as evidenced by the shifting of the Ag peaks to higher 2θ values. However, the fact that two distinct peaks are present indicates that a single phase alloy has not formed. A sample held at 450 °C for 84 h also contained two distinct peaks rather than a single peak expected for a homogeneous 75 Pd/25 Ag alloy. After 102 h at 500 °C the single phase alloy had not yet completely formed, as indicated by the distinct shoulders remaining in the diffraction peaks. After 64 h at 550 °C a single phase palladium–silver alloy was formed.

Fig. 11 shows expanded X-ray diffraction data for the homogeneous Pd–Ag alloy formed at 550 °C, including diffraction angles of all the major lattice planes of low Miller index of the alloy's face centered cubic structure. Table 2 lists the measured *d*-spacing between the fcc (1 1 1) planes and the

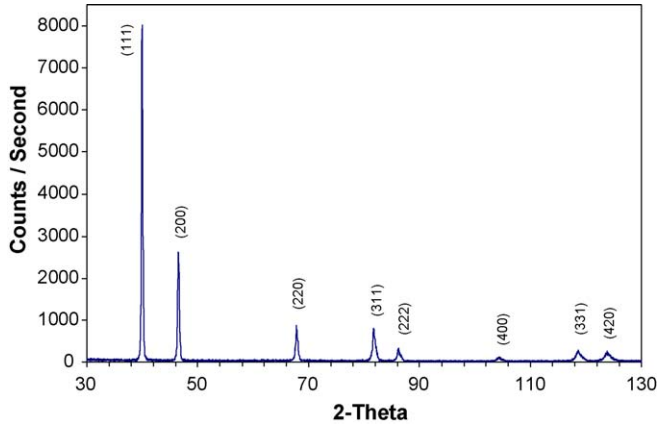

Fig. 11. Expanded X-ray diffraction data for a homogeneous alloy of 75 at.% Pd and 25 at.% Ag with the fcc crystal structure.

Table 2
The (1 1 1) *d*-spacing and fcc cube-edge lattice parameters for pure Pd and Ag and the $Pd_{0.75}$ $Ag_{0.25}$ alloy

	(1 1 1) *d*-spacing (Å)	fcc cube-edge lattice parameter (Å)
Pd	2.246	3.89
Ag	2.359	4.09
Pd/Ag	2.255	3.91

fcc cube edge lattice parameters for pure Pd, Ag, and the prepared Pd/Ag alloy. The *d*-spacing between the (1 1 1) planes and the calculated lattice parameter for the fcc Pd/Ag alloy correspond well with reported literature values for a 75/25 palladium–silver alloy [19].

In efforts to lower the temperature for interdiffusion, five alternating layers of palladium and silver were deposited with the same total mass and thickness as the three layer deposition. Fig. 12 shows X-ray diffraction data comparing the three and five layer deposition after annealing at 400 °C. Fig. 12 shows that, whereas after 125 h at 400 °C the three layer deposition still contained distinct diffraction peaks for silver and palladium phases, the pattern for the five layer deposition heated for 100 h at 400 °C contained only single diffraction peaks with minor shoulders, indicating that a homogeneous palladium–silver alloy had almost completely formed.

Alloys of 80 wt.% Pd–20 wt.% Cu ($Pd_{2.39}Cu_1$) and 60 wt.% Pd–40 wt.% Cu ($Pd_1Cu_{1.12}$) were also prepared. The Pd 80 wt.%–Cu 20 wt.% alloys show only a face centered cubic crystal structure. The 60 wt.% Pd–40 wt.% Cu alloys undergo a phase transformation between fcc to bcc at temperatures below 598 °C. Such palladium–copper alloys have a long history in hydrogen transport membrane research [14,25–28] and are under investigation for tolerance to sulfur.

6. Tolerance of hydrogen transport membrane catalysts to compounds of sulfur

Hydrogen permeation results reviewed above have referred to feeds in the absence of compounds of sulfur. Sulfur is a

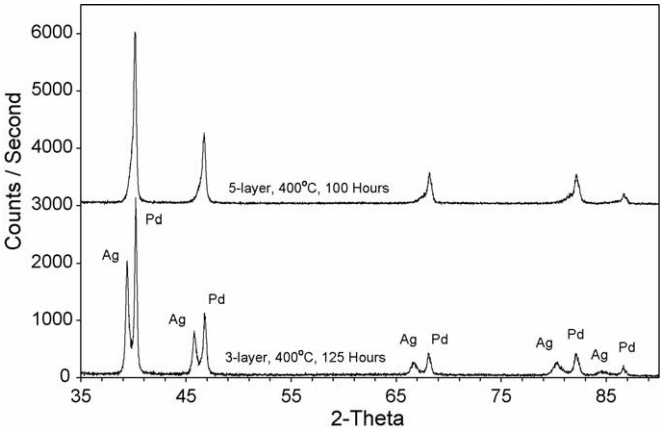

Fig. 12. X-ray diffraction data showing enhanced interdiffusion of Pd and Ag starting with five alternating layers of deposited Pd and Ag relative to three layers.

Table 3
Calculated concentrations of H_2S required to transform Pd to Pd_4S

Temperature (°C)	Temperature (K)	Maximum H_2S Tolerated (in ppmv) before formation of Pd_4S					
		~100% H_2	60% H_2	40% H_2	20% H_2	10% H_2	1% H_2
220	493	0.0259	0.0155	0.0104	0.00518	0.00259	0.000259
250	523	0.0704	0.0422	0.0282	0.0141	0.00704	0.000704
300	537	0.296	0.178	0.119	0.0593	0.0297	0.00297
325	598	0.556	0.333	0.222	0.111	0.0555	0.00555
350	623	0.990	0.594	0.396	0.198	0.0990	0.00990
375	648	1.69	1.01	0.673	0.337	0.168	0.00168
400	673	2.77	1.66	1.11	0.553	0.277	0.00277
425	698	4.38	2.63	1.75	0.877	0.438	0.00438
450	713	5.67	3.40	2.23	1.13	0.567	0.00567
500	773	14.5	8.70	5.80	2.90	1.45	0.145
550	823	28.5	17.1	11.4	5.7	2.85	0.285
600	873	51.9	31.1	20.6	10.3	5.16	0.516
700	973	143	85.9	57.2	28.6	14.3	1.43
800	1073	327	196	131	65.3	32.7	3.27
900	1173	647	388	259	129	64.7	6.47

$4Pd + H_2S \rightleftarrows Pd_4S + H_2$, $\Delta G^\circ = -71.613$ kJ/mol. Assumes ΔG_f° of $H_2S = -33.56$ kJ/mol and ΔG_f° of $Pd_4S = -105.173$ kJ/mol. $-\Delta G^\circ/RT = \ln K$.

well-established poison for palladium catalysts [29]. Minor quantities of compounds of sulfur not only poison the palladium surface, but also convert palladium into bulk sulfides including especially Pd_4S [2,29]. Table 3 lists calculated concentrations of H_2S in the feed which will convert palladium into Pd_4S as a function of temperature and hydrogen concentration in the feed based upon the equilibrium of $4Pd + H_2S = Pd_4S + H_2$ where the equilibrium constant, K, is equal to $[H_2]/[H_2S]$. For conditions of interest in industrial high-temperature water-gas shift reactors (320–440 °C; $[H_2] < 40$ mol%), even a few parts per *billion* by volume H_2S will be sufficient to poison unalloyed palladium catalysts according to these simple equilibrium thermodynamic calculations.

Fig. 13 shows the rapid decrease in hydrogen flux through an unalloyed palladium foil exposed to 20 ppmv H_2S at 320 °C in the presence of 60 mol% H_2 in the feed. (Note at very high concentration of H_2, higher tolerance to H_2S is achieved, but is not likely to be of practical value. See Table 3.) X-ray diffraction data of the palladium membrane after exposure to H_2S shown in Fig. 14 shows the absence of metallic palladium and confirms formation of Pd_4S. Unalloyed palladium membranes are eventually destroyed by sulfur as the palladium converts into bulk sulfide. It should be stressed that the poisoning of unalloyed palladium is more than simple adsorption of sulfur blocking surface sites. A thick layer (5–10 μm) of palladium is converted into Pd_4S after 5 days operation.

Palladium–silver alloys, although possibly preferred on the membrane permeate side in the absence of sulfur, cannot be used on the retentate-side of membranes if sulfur is present. Fig. 15 shows the very rapid decrease in hydrogen flux of a 75 at.% Pd–25 at.% Ag membrane exposed to only 10 ppmv H_2S at 320 °C with 80 mol% H_2 in the feed. Fig. 16 shows X-ray diffraction data of the membrane surface after only ~3 days of exposure to H_2S suggesting formation of a bulk silver–palladium sulfide ($Ag_5Pd_{10}S_5$, according to JCPDF–International Center for Diffraction Data, #27-1156). Palladium–silver alloys are not recommended if membranes are to be exposed to sulfur.

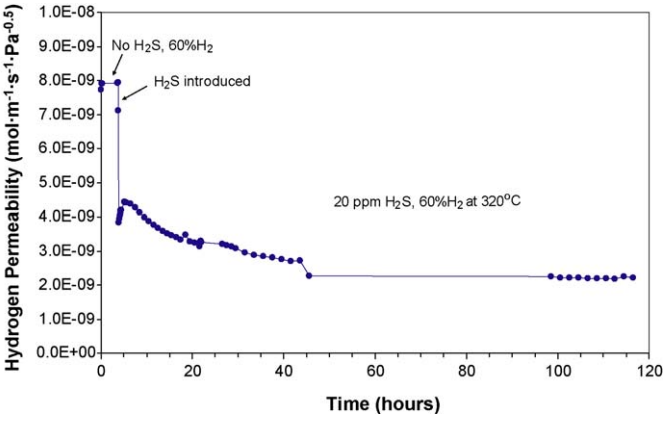

Fig. 13. Poisoning of an unalloyed palladium foil by 20 ppmv H_2S at 320 °C.

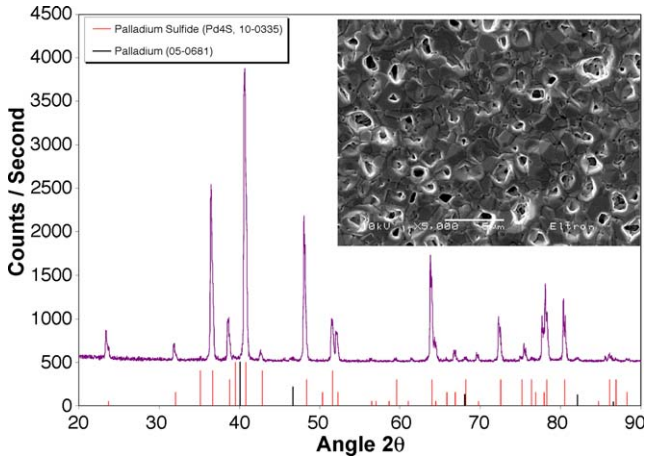

Fig. 14. X-ray diffraction data confirming conversion of an unalloyed palladium into bulk Pd_4S. Unalloyed palladium cannot be used with membranes exposed to sulfur. Insert shows SEM image of the membrane surface which was exposed to H_2S.

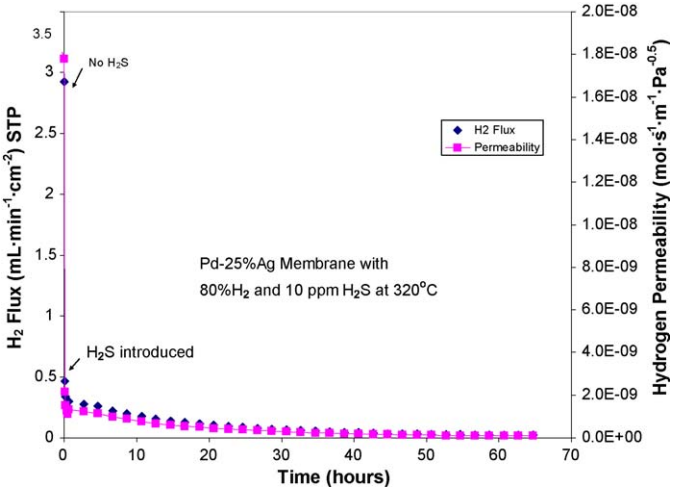

Fig. 15. Rapid poisoning of a 75 at.% palladium–25 at.% silver membrane upon exposure to 10 ppmv H_2S at 320 °C. Such alloys cannot be used with membranes exposed to sulfur.

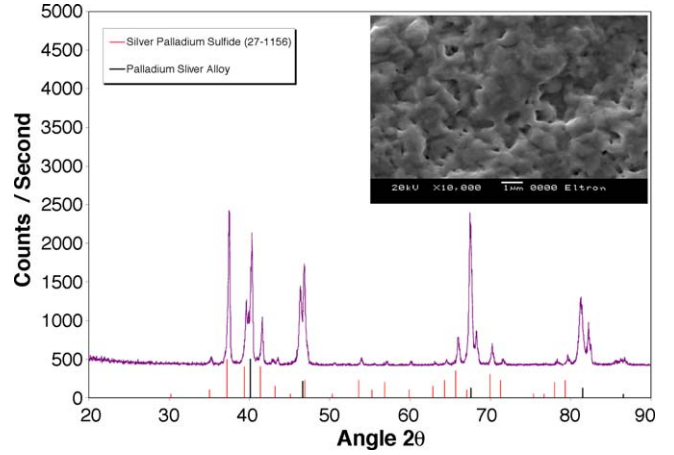

Fig. 16. X-ray diffraction data of a palladium–silver alloy membrane surface showing formation of a bulk silver–palladium sulfide.

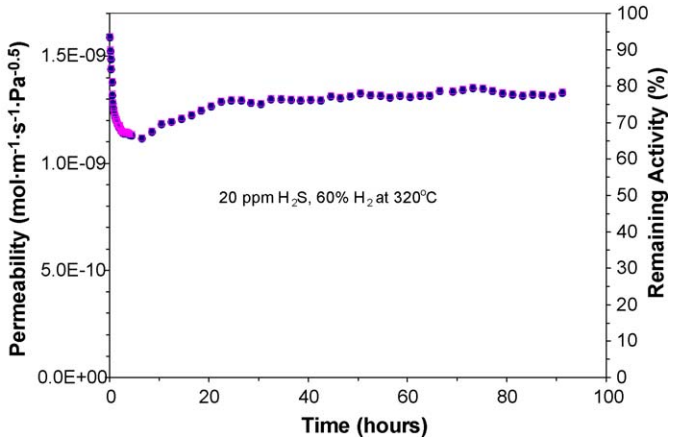

Fig. 17. Effect of 20 ppmv H_2S on a membrane containing 80 wt.% Pd and 20 wt.% Cu at 320 °C and 60 mol% H_2 in the feed.

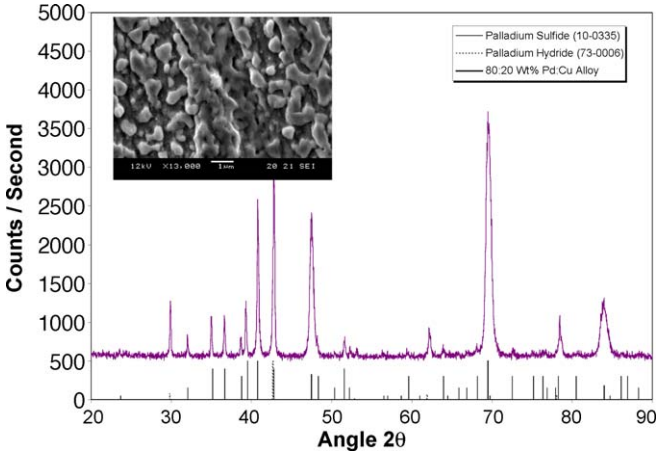

Fig. 18. X-ray diffraction pattern showing that a fraction of 80 wt.% Pd–20 wt.% Cu alloy did not completely transform into bulk sulfides, although Pd_4S was also formed.

Fig. 17 shows the effect of 20 ppmv H_2S on a membrane composed of 80 wt.% Pd and 20 wt.% Cu at 320 °C with a feed containing 60 mol% H_2. This alloy showed slightly better tolerance to sulfur relative to unalloyed Pd or the Pd–Ag alloy, although it was not completely satisfactory. Fig. 18 shows that some bulk Pd_4S formed, although most of the alloy remained. Unlike unalloyed palladium and Pd–Ag alloys, some of the copper–palladium alloys resist formation of bulk sulfides and retain their metallic luster after exposure to H_2S at ppm levels [25–27]. As illustrated in Fig. 18, both X-ray diffraction and scanning electron microscopy analysis of the Pd–Cu alloy membrane indicate that a significant fraction of the near surface region remains as the metallic alloy, although bulk palladium sulfide has formed as well. These results were consistent with the permeation study (Fig. 17), which shows that the Pd–Cu membrane retains ∼80% of its original permeability upon exposure to 20 ppmv H_2S, with 60% H_2 at 320 °C.

Table 4
Calculated minimum ΔG_f for palladium alloys or intermetallic compounds needed to avoid bulk sulfide formation with 20 ppmv H_2S in feed (kJ/mol)

Temperature (°C)	Temperature (K)	20 ppm H_2S in feed				
		60% H_2	40% H_2	20% H_2	10% H_2	1% H_2
220	493	−7.3	−7.8	−8.5	−9.2	−10.8
400	673	−3.5	−4.1	−5.0	−6.0	−8.2
500	773	−1.3	−1.9	−3.1	−4.2	−6.8
600	873	+1.1	+0.08	−1.2	−2.5	−5.4

Table 5
Estimated surface free energies of sulfur bound to metals

Surface	ΔG (kJ/mol)
Pd (1 1 1)	468
Cu (1 1 1)	427
Ag (1 1 1)	351
Pd_3Cu (1 1 1)	457
PdCu (1 1 0)	459
Pd_3Ag (1 1 1)	474

Table 6
Calculated equilibrium pressures and concentrations of H_2S with ZnS in steam

T (°C)	K_P—sphalerite	P_{H_2S} (bar)	H_2S (ppmv)	K_P—wurtzite	P_{H_2S} (bar)	H_2S (ppmv)
300	7.24×10^6	1.49×10^{-6}	0.051	4.37×10^5	2.47×10^{-5}	0.852
325	3.75×10^6	2.91×10^{-6}	0.100	2.55×10^5	4.24×10^{-5}	1.46
350	2.05×10^6	5.35×10^{-6}	0.184	1.55×10^5	6.97×10^{-5}	2.40
375	1.18×10^6	9.15×10^{-6}	0.316	9.87×10^4	1.09×10^{-4}	3.76
400	7.08×10^5	1.53×10^{-5}	0.528	6.49×10^4	1.66×10^{-4}	5.72
425	4.41×10^5	2.45×10^{-5}	0.845	4.41×10^4	2.45×10^{-4}	8.45
450	2.85×10^5	3.79×10^{-5}	1.31	3.08×10^4	3.51×10^{-4}	12.1

K_P values adapted from Twigg et al. [10]; steam = 10.8 barg, 0.373 mol fraction at 29 bara; $H_2S + ZnO = ZnS + H_2O$; $[H_2S] = K_P[H_2O]$.

In a search for more sulfur resistant palladium alloys and intermetallic compounds [30], it is instructive as a first step to consider the thermodynamics of bulk sulfide formation. Calculations summarized in Table 4 imply that if alloys or intermetallic compounds with ΔG_f can be found with values just in excess of -5 to -10 kJ mol^{-1}, they can resist formation of bulk sulfides. Research is currently underway to develop and test new palladium alloys and intermetallic compounds.

Resistance to formation of bulk sulfides is a necessary, although not sufficient criterion for resistance to poisoning by sulfur. Poisoning can also occur by adsorption of a monolayer of sulfur on surfaces even if bulk sulfides do not form. Table 5 shows estimated surface free energies of sulfur bound to various metals and alloys of interest in membrane research, based upon the work of Alfonso, Cugini and Sholl [31]. The very high binding energies for adsorption of sulfur imply that even if some of the copper–palladium alloys do not form bulk sulfides, that sulfur is almost certainly adsorbed on the surface. If this is true, and if membranes continue to function, it implies that the surface sulfides of Pd–Cu alloys must retain some catalytic activity for hydrogen dissociation, as in cobalt–molybdenum catalysts which function while sulfided.

Table 6 shows calculated values of H_2S which are predicted to escape guard beds of ZnO in the presence of steam at equilibrium for the reaction $H_2S + ZnO = H_2O + ZnS$. Catalysts must be tolerant to these values of H_2S if used with current guard beds of ZnO.

7. Conclusions

Oxygen transport membranes can be integrated with water-gas shift reactors and hydrogen separation membranes for the production of ultra-high purity hydrogen from natural gas. Sulfur and other potential catalyst poisons need to be removed from natural gas before the reforming steps. In the membrane reactors, natural gas is converted into synthesis gas by a combination of steam reforming and oxidation reactions run under conditions above 900 °C which overwhelmingly favor production of $H_2 + CO$ at equilibrium. In the production of hydrogen from coal, management of impurities and potential catalyst poisons is key to success. In the presence of steam in the temperature range between 340 and 440 °C, encountered in the exhaust of water-gas shift reactors, commercial adsorbents such as ZnO can at best reduce levels of H_2S to about 2 to 10 ppmv. Hydrogen dissociation catalysts on surfaces of hydrogen transport membranes must be resistant to this level of H_2S. Unalloyed palladium and conventional palladium–silver alloys appear to be especially vulnerable to poisoning by sulfur and are not recommended for use in hydrogen transport membranes exposed to compounds of sulfur. Other palladium alloys and intermetallic compounds which do not form bulk sulfides appear key to production of sulfur-resistant hydrogen dissociation catalysts for use on hydrogen purification membranes. Membranes may offer a potential means for economic sequestration of CO_2 [32].

Acknowledgements

We acknowledge the Department of Energy which supported this work under the DOE SBIR and DOE Vision 21 programs, and under contracts DE-FC26-00NT40762, DE-FC26-97FT96052, DE-FG02-04ER83934, DE-FG02-04ER83935 and DE-FC26-01NT41145. Any findings, conclusions or recommendations expressed herein are those of the authors and do not necessarily reflect the views of the DOE.

References

[1] F.S. Galasso, Structure, Properties and Preparation of Perovskite-Type Compounds, Pergamon Press, Oxford, 1969.
[2] A.F. Wells, Structural Inorganic Chemistry, 5th ed., Clarendon Press, Oxford, 1984.
[3] C. Kittel, Introduction to Solid State Physics, 3rd ed., Wiley, New York, 1967, p. 404.
[4] A.F. Sammells, M.V. Mundschau (Eds.), Nonporous Inorganic Membranes, Wiley–VCH, New York, 2006.
[5] R.J.H. Voorhoeve, J.P. Remeika, L.E. Trimble, in: R.L. Klimisch, J.G. Larson (Eds.), The Catalytic Chemistry of Nitrogen Oxides, Plenum, New York, 1975, pp. 215–233.
[6] P.A. Cox, Transition Metal Oxides, Clarendon Press, Oxford, 1995.
[7] J.B. Goodenough (Ed.), Localized to Itinerant Electronic Transition in Perovskite Oxides, Springer, Berlin, 2001.
[8] N. Tsuda, K. Nasu, A. Fujimori, K. Siratori, Electronic Conduction in Oxides, Springer, Berlin, 2000.
[9] V.E. Henrich, P.A. Cox, The Surface Science of Metal Oxides, Cambridge University Press, Cambridge, 1996, pp. 36–42.
[10] M.V. Twigg (Ed.), Catalyst Handbook, 2nd ed., Manson Publishing, London, 1997.
[11] M.V. Mundschau, X. Xie, A.F. Sammells, in: D.C. Thomas (Ed.), Carbon Dioxide Capture for Storage in Deep Geologic Formations—Results from the CO_2 Capture Project, vol. 1, Elsevier, Amsterdam, 2005 , pp. 291–306 (Chapter 16).

[12] S. Glasstone, Textbook of Physical Chemistry, 2nd ed., Van Nostrand, New York, 1951, p. 432.
[13] E. Raask, Mineral Impurities in Coal Combustion, Hemisphere Publishing Corporation/Springer, Washington, DC/Berlin, 1985.
[14] S.N. Paglieri, J.D. Way, Sep. Purif. Meth. 31 (1) (2002) 1–169.
[15] K. Christmann, Surface Physical Chemistry, Steinkopff Verlag/Springer, Darmstadt/New York, 1991.
[16] J.B. Benzinger, in: E. Shustorovich (Ed.), Metal-Surface Reaction Energetics, VCH, Weinheim, 1991 , pp. 53–107 (Chapter 2).
[17] J.B. Hunter, US Patent 2,773,561 (11 December, 1956).
[18] A.C. Makrides, M.A. Wright, D.N. Jewett, US Patent 3,350,846 (7 November, 1967).
[19] B. McCool, G. Xomeritakis, Y.S. Lin, J. Membr. Sci. 161 (1999) 67–76.
[20] Y. Zhang, T. Ozaki, M. Komaki, C. Nishimura, J. Membr. Sci. 224 (2003) 81–91.
[21] Y. Zhang, T. Ozaki, M. Komaki, C. Nishimura, J. Alloy. Compd. 356–357 (2003) 553–556.
[22] Y.S. Cheng, K.L. Yeung, J. Membr. Sci. 158 (1999) 127–141.
[23] R.E. Buxbaum, P.C. Hsu, US Patent 5,149,420 (September 22, 1992).
[24] R.W. Berry, P.M. Hall, M.T. Harris, Thin Film Technology, Van Nostrand Reinhold, New York, 1968.
[25] D.L. McKinley, US Patent 3,350,845 (7 November, 1967).
[26] D.L. McKinley, US Patent 3,439,474 (22 April, 1969).
[27] B.D. Morreale, M.V. Ciocco, B.H. Howard, R.P. Killmeyer, A.V. Cugini, R.M. Enick, J. Membr. Sci. 241 (2004) 219–224.
[28] A. Kulprathipanja, G.O. Alptekin, J.L. Falconer, J.D. Way, J. Membr. Sci. 254 (2005) 49–62.
[29] H.W. Lohse, Catalytic Chemistry, Chemical Publishing Company, Brooklyn, 1945.
[30] E. Savitsky, V. Polyakova, N. Gorina, N. Roshan, Physical Metallurgy of Platinum Metals, Mir Publishers, Moscow, 1978.
[31] D.R. Alfonso, A.V. Cugini, D.S. Sholl, Surface Sci. 546 (2003) 12–26.
[32] M.V. Mundschau, X. Xie, A.F. Sammells, in: E.S. Rubin, D.W. Keith, C.F. Gilboy (Eds.), Proceedings of the Seventh International Conference on Greenhouse Gas Control Technologies, vol. I, Elsevier, Amsterdam, 2005, pp. 93–101.